



**HAL**  
open science

## Superconducting cryo-magnets processed by Spark Plasma Sintering and Texturing

Jacques Noudem, Louis Dupont, Pierre Bernstein, Richard Retoux, Geoffroy Chevallier, Claude Estournes, Kévin Berger, Muralidhar Miryala, Masato Murakami

### ► To cite this version:

Jacques Noudem, Louis Dupont, Pierre Bernstein, Richard Retoux, Geoffroy Chevallier, et al.. Superconducting cryo-magnets processed by Spark Plasma Sintering and Texturing. Giacomo Cao; Claude Estournes; Javier Garay; Roberto Orru. Spark Plasma Sintering: Current Status, New Developments and Challenges, 1st Edition, Elsevier, Chapter 8, pp. 185-199, 2019, 9780128177440. 10.1016/B978-0-12-817744-0.00008-8 . hal-01988782

**HAL Id: hal-01988782**

**<https://hal.science/hal-01988782>**

Submitted on 8 Apr 2024

**HAL** is a multi-disciplinary open access archive for the deposit and dissemination of scientific research documents, whether they are published or not. The documents may come from teaching and research institutions in France or abroad, or from public or private research centers.

L'archive ouverte pluridisciplinaire **HAL**, est destinée au dépôt et à la diffusion de documents scientifiques de niveau recherche, publiés ou non, émanant des établissements d'enseignement et de recherche français ou étrangers, des laboratoires publics ou privés.





## Open Archive Toulouse Archive Ouverte (OATAO)

OATAO is an open access repository that collects the work of Toulouse researchers and makes it freely available over the web where possible

This is a Publisher's version published in: <http://oatao.univ-toulouse.fr/24658>

**Official URL:** <https://doi.org/10.1016/B978-0-12-817744-0.00008-8>

### **To cite this version:**

Noudem, Jacques G. and Dupont, Louis and Bernstein, Pierre and Retoux, Richard and Chevallier, Geoffroy  and Estournès, Claude  and Bergeron, Keith and Higuchi, Masaaki and Muralidhar, Miryala and Murakami, Masato *Superconducting cryo-magnets processed by spark plasma sintering and texturing*. (2019) In: Spark Plasma Sintering. Elsevier, 185-199. ISBN 978-0-12-817744-0

Any correspondence concerning this service should be sent to the repository administrator: [tech-oatao@listes-diff.inp-toulouse.fr](mailto:tech-oatao@listes-diff.inp-toulouse.fr)

## CHAPTER 8

# Superconducting cryo-magnets processed by spark plasma sintering and texturing

J. Noudem<sup>\*</sup>, L. Dupont<sup>\*</sup>, P. Bernstein<sup>\*</sup>, R. Retoux<sup>\*</sup>, G. Chevallier<sup>†</sup>, C. Estournès<sup>†</sup>, K. Berger<sup>‡</sup>, M. Higuchi<sup>§</sup>, M. Muralidhar<sup>§</sup>, M. Murakami<sup>§</sup>

<sup>\*</sup>Normandie Univ, ENSICAEN, UNICAEN, CNRS, CRISMAT, Caen, France

<sup>†</sup>CIRIMAT, Université de Toulouse; CIRIMAT, CNRS, Université Toulouse III—Paul Sabatier, Toulouse, France

<sup>‡</sup>GREEN, University of Lorraine, Vandoeuvre-lès-Nancy Cedex, France

<sup>§</sup>Superconducting Materials Laboratory, Graduate School of Science & Engineering, Shibaura Institute of Technology, Tokyo, Japan

## 1. Introduction

Since the discovery of high temperature superconductivity (HTS) [1], intensive research has been devoted to discovering new materials [2–9], in order to improve the superconducting properties [10–16] and/or develop different devices such as permanent magnets, motors, and flywheel energy storage for potential applications [17–24].

Most of the elaboration processes for polycrystalline samples are based on classical solid-state reactions relying, basically, on conventional sintering [25]. Powder melt process [26], melt texture growth [27] or top seed melt texture growth [11,16,28], hot pressing [12], sinter-forging [29], and application of a magnetic field [30] are also used to densify and/or to induce grain orientation. Otherwise, the novel Spark Plasma Sintering (SPS) technique has been developed, and is commonly used nowadays to prepare various materials [31–34]. SPS is a unique sintering method combining mechanical pressure and high current pulses or DC current as the heating source for sintering [35,36]. The mixed raw material is directly poured into a die assembly made of electrically conductive materials, without any additive or binder, and pressed uniaxially by punches holding the powder compact, while the current is supplied to the die assembly. One of the main advantages of the SPS technique is the rapid densification of various materials in a very short time (a few minutes) as compared to the Conventional Sintering (CS) method.

The purpose of this chapter is to describe the fabrication conditions for: (i) texturing lamellar  $\text{Bi}_2\text{Sr}_2\text{CaCu}_2\text{O}_8$  (Bi:2212) by the spark plasma texturing-SPT method; and (ii) densifying granular  $\text{MgB}_2$ ; to investigate their mechanical properties and discuss their superconducting properties and performance.

## 2. Experimental procedure

The  $\text{MgB}_2$  bulks were prepared with an SPS device (FCT Systeme GmbH, HD25, Rauenstein, Germany) in DC mode. Different powders were used as starting materials: (i) commercial  $\text{MgB}_2$  powder (PAVEZYUM, Advanced Chemicals, Turkey); (ii) the ex-situ mixing powder magnesium (Mg) and nano boron (B) powders; and (iii) the mixture of Mg and carbon-encapsulated boron powders. The processing conditions are detailed elsewhere [37]. Basically, the  $\text{MgB}_2$  powder is put into a graphite die of 20 mm diameter and sintered for 20 min in dynamic vacuum from 800°C to 950°C with current pulses in the 2 kA range, while applying uniaxial pressure up to 100 MPa.

Additional processing was carried out using another Spark Plasma Sintering system (namely Dr. Sinter SPS 2080, Sumitomo Coal Mining Co., Ltd., Japan) and the following steps. The powder was introduced into the tungsten carbide (WC) die (20 mm diameter), then placed into the working chamber under vacuum. The temperature was increased (100°C/min) up to the chosen sintering value from 600°C to 800°C while a load of 500 MPa was applied during 20 min with a sequence of 12on-2off pulses.

Basically, different series of samples have been prepared. The first series is focused on the role of studying the precursor powder on the superconducting properties. Three sets of bulk  $\text{MgB}_2$  material were processed from: (i) commercial available powder; (ii) a mixture of Mg metal and amorphous B using a single-step solid-state reaction process; and (iii) a mixture of amorphous boron coated with carbon and Mg metal. The second series was related to highly densifying the samples using tungsten carbide molds at various temperatures and comparing their properties to the optimized sample obtained from a graphite mold at 950°C. The third series (Table 3) of sample are  $\text{MgB}_2$  discs prepared with different diameters and thicknesses. The final batch of samples, listed in Table 4, was consolidated at different sintering temperatures for mechanical property investigations. In the next section, we use the following terms:

- S1, the sample prepared by conventional sintering;
- S2a, the SPS sample consolidated from the  $\text{MgB}_2$  powder using graphite mold at 850°C;

- S2b, the SPS sample consolidated from the  $\text{MgB}_2$  powder using graphite mold at  $950^\circ\text{C}$ ;
- S3, the SPS sample prepared from the mixture of Mg + B using graphite mold at  $850^\circ\text{C}$ ;
- S4, the SPS sample prepared from the mixture of Mg + B/C using graphite mold at  $850^\circ\text{C}$ ;
- S5, the SPS sample made from  $\text{MgB}_2$  powder densified at high pressure using a WC mold at  $800^\circ\text{C}$ ; and
- S6 and S7, the SPS samples made from  $\text{MgB}_2$  powder densified at high pressure using a WC mold at 700 and  $750^\circ\text{C}$ , respectively.

For the  $\text{Bi}_2\text{Sr}_2\text{CaCu}_2\text{O}_8$  (Bi:2212), the powder was prepared from oxides and carbonates precursors by using conventional solid-state reaction. The powder was cold pressed uni-directionally at 60 MPa into pellets with a diameter of 13 mm. The pellets were conventionally sintered at  $700^\circ\text{C}$  for 2 h in air and placed at the center of a 20 mm diameter graphite die, in order to ensure the free deformation and texturing process described elsewhere [38, 39]. The final processing was carried out using an FCT HD-25 Spark Plasma Sintering machine. Electric current pulses (2000 A, 4 V) were passed through the sample in a vacuum ( $10^{-3}$  bar) for a duration of 10 min, heating the samples at  $750^\circ\text{C}$ , while a uniaxial pressure of 50 MPa was applied. During this stage of the process, the temperature, the applied pressure, and the displacement or shrinkage of the sample was recorded. After this, the samples were heated at  $750^\circ\text{C}$  for 2 h in air to ensure the desired stoichiometry.

The density of the prepared samples was determined by using Archimedes' method (KERN & Sohn GmbH, Baligen, Germany) in de-ionized water.

Phase identification was achieved by X-Ray diffraction using an X'Pert Powder diffractometer in the Bragg-Brentano geometry. Microstructural analysis was performed on fracture surfaces containing the pressing axis during processing, with a Carl Zeiss (Supra 55, Oberkochen, Germany) scanning electron microscope (SEM) in backscattering electron (BSE) mode. Otherwise, transmission electron microscopy (TEM) was used to investigate the finer microstructural features. The TEM study was performed using a 200 kV JEOL 2010 FEG transmission electron microscope fitted with a double tilt sample holder (tilt  $\pm 42^\circ$ ). The cationic composition of the materials was determined by Energy Dispersive X-ray analysis (EDX) using EDAX analyzers coupled with the microscope. The sample was ordered to prevent any damage.

Cubic-shaped samples of  $2 \times 2 \times 2 \text{ mm}^3$  were cut from the processed samples by using a low speed diamond saw (Struers, Champigny sur Marne, France), for physical characterization.

The magnetic moment versus temperature (M-T) and the magnetization hysteresis loops (M-H loops) at 20 K between  $-5$  and  $+5$  T were measured with a SQUID magnetometer (Quantum Design, model MPMS5). The critical temperature ( $T_c$ ) as well as the critical current ( $J_c$ ) of the samples were deduced from these measurements. Using Bean's critical model [40], the  $J_c$  values were derived from the equation:

$$J_c = \frac{20\Delta M}{a \left(1 - \frac{a}{3b}\right)} \quad (1)$$

where

$\Delta M$  is the difference in magnetization between increasing and decreasing magnetic field; and.

$a(1 - (a/3b))$  is a geometric factor related to the sample dimensions with  $a < b$ .

Trapped field measurements were carried out at 20 K on a stack of two 20 mm diameter disc-shaped samples using two Hall effect cryogenic sensors located (i) at the center of the upper surface of the stack and (ii) between the two pellets. The overall thickness of the stack was 20 mm. The samples were magnetized by field cooling (FC) in a magnetic field of 3 T (superconducting coil, Oxford Instruments IPS 120-10) and then the applied field was decreased to  $-3$  T at a rate of 0.10 T/min to avoid any flux jump. The average temperature of the stack was measured using two Cernox thermometers mounted on the upper and the lower surfaces of the sample holder. Further details on the experimental setup are reported elsewhere [41].

### 3. Results and discussion

#### 3.1 MgB<sub>2</sub> superconductor SPS densified

X-ray diffraction (XRD) patterns at room temperature of the sample (S2b) processed at 950°C has been carried out (Fig. 1). The diffraction peaks of the samples can be indexed as a hexagonal structure in space group P6/mmm. Lattice parameters were calculated and are shown in Table 1. The lattice parameters do not show any significant variation with respect to the theoretical values. The XRD of the sample prepared at 950°C shows that the major peaks are related to the MgB<sub>2</sub> phase with traces of MgO, which was already present in the as-supplied commercial MgB<sub>2</sub> powder, as can

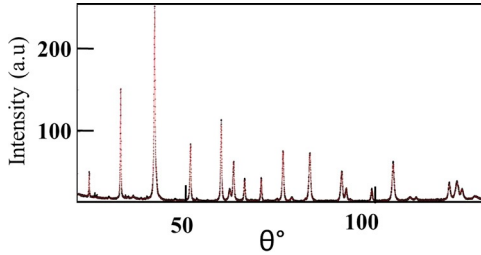


**Fig. 1** XR-diffraction XRD patterns of sample prepared at 950°C.

**Table 1** Lattice parameters

Cell parameters	a (Å)	b (Å)
Theory	3.085	3.085
Measurements	3.08518(5)	3.08518(5)

be seen in Fig. 1. This figure also reveals the presence of  $\text{MgB}_4$  as reported elsewhere [42, 43–46]. According to the phase diagram of the Mg-B system [47] at high temperature, the Mg vapor can be in equilibrium with  $\text{MgB}_2$  as well as with  $\text{MgB}_4$ .

The bulk densities are 60, 68, 76, 85, and 96% from the theoretical density of  $2.62 \text{ g/cm}^3$  calculated from XRD patterns for S1, S2, S3, S4, and S5 samples, respectively. As expected, sample S5 fabricated using WC tool is more dense. Fig. 2 shows the SEM micrographies from the fractured cross sections of the samples S1, S2, S3, S4, and S5. The conventional sintering (CS) specimen (Fig. 2A) contains more pores than the SPS specimens, in accordance with the densities values reported above. However, sample S5, prepared at high pressure, shows more compact and large grains than the other samples processed by SPS. The grain growth under high pressure can be clearly observed (Fig. 2D). The samples S3 and S4 show a homogeneous microstructure with a narrow grain size distribution (Fig. 2B and C). In order to confirm the small grain size of the sample prepared using nano boron powder, TEM observations, shown in Fig. 3, were carried out on an ion sliced sample of S4. The homogeneous grain size distribution is clearly seen, with most grains presenting a size ranging from 30 to 80 nm.

The temperature dependence of the magnetic moments of samples S1, S2a, S2b, S3, S4, and S5 measured applying a 10 Oe field shows (Fig. 4) a narrow transition with an onset around 38, 5 K. However, for sample S4, we have  $T_c = 35 \text{ K}$ . A possible explanation is the partial substitution of boron by carbon in S4.

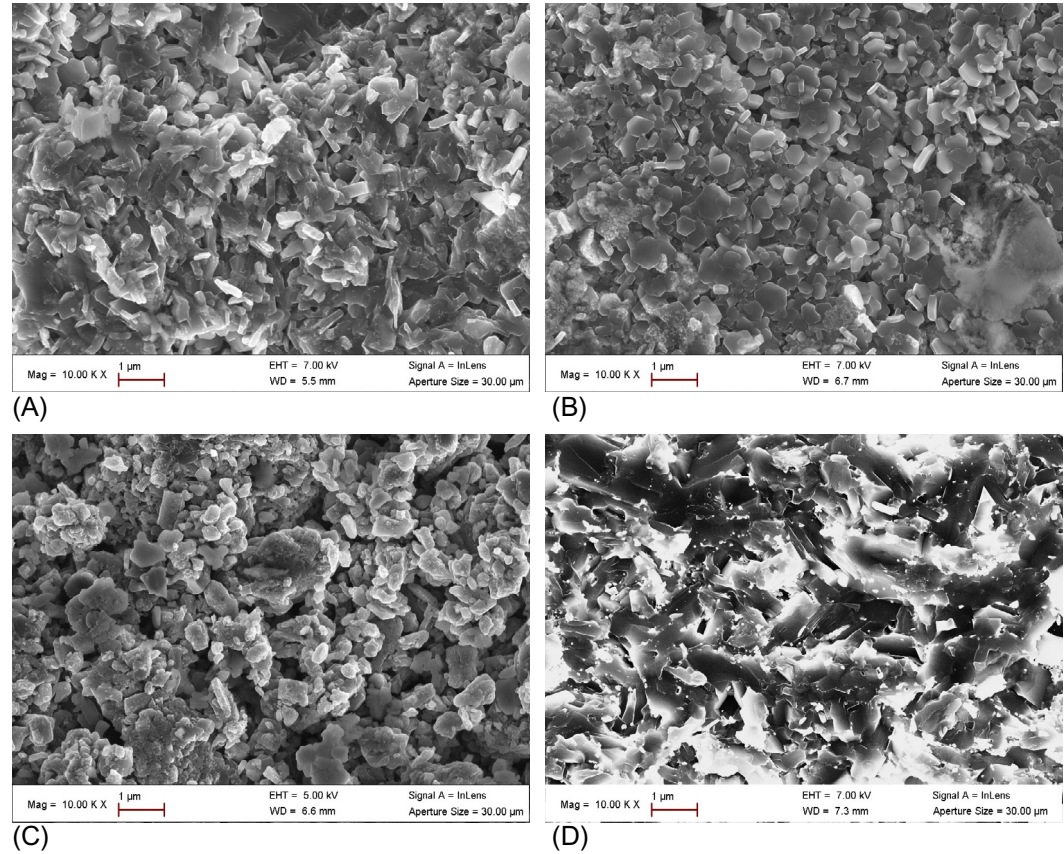


**Fig. 2** SEM micrographs of different samples (A) conventional sintering, (B) SPS at 850°C with Mg + B addition, (C) SPS graphite mold at 950°C, and (D) SPS/WC mold at 800°C.



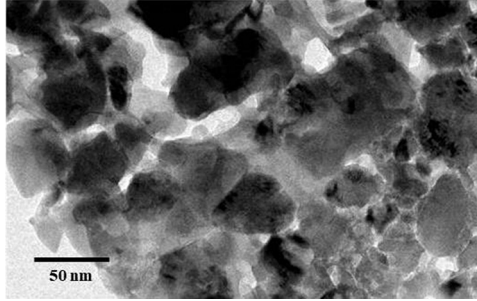


Fig. 3 TEM micrograph of the Mg+B sample confirming the small grain size.

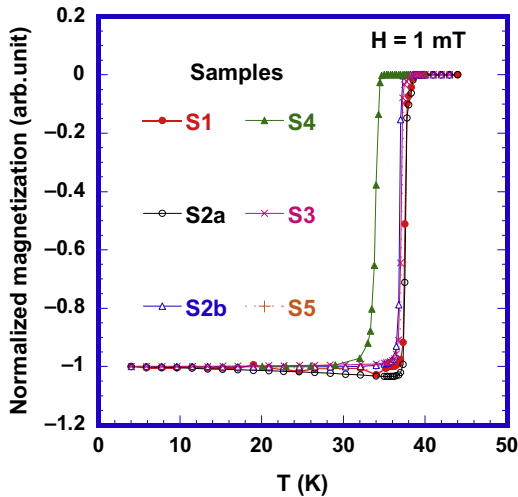
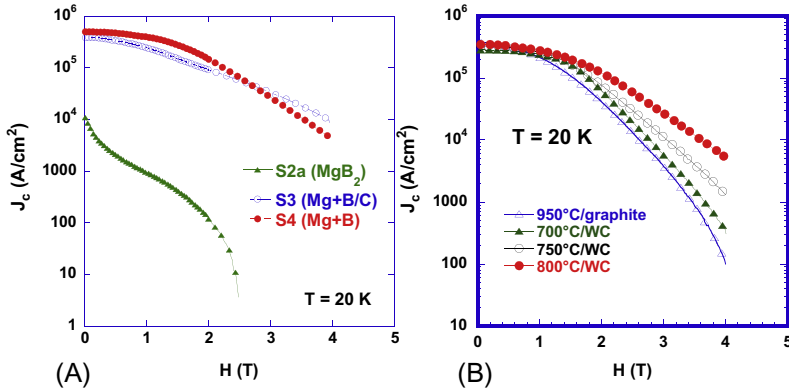


Fig. 4 Normalized magnetic moment of the different samples.

Fig. 5 shows the critical current density as a function of magnetic field for two series of samples at 20 K. It is clear that, high  $J_c$  values are obtained with samples S3 and S4, i.e., the sample with a mixture of Mg metal and amorphous B and the carbon-encapsulated boron one. We observe that while the  $J_c$  of S4 is slightly lower than that of S3 in the domain ranging from the self-field to 2.5 T, above 2.5 T there is a cross over and  $J_c$  for S3 is higher than  $J_c$  for S4. This cross over is important for the practical applications of the compound. Now let's compare samples S3 and S4 with sample S2a, prepared in the same conditions using commercial powder. The  $J_c$  of sample S2 is much smaller than that of S3 and S4. There are two main explanations. Firstly, sample S2a is more porous than S3 and S4. Its relative density is only



**Fig. 5**  $J_c$ - $H$  curves at 20 K of the samples obtained (A) from different powders and (B) various processing conditions.

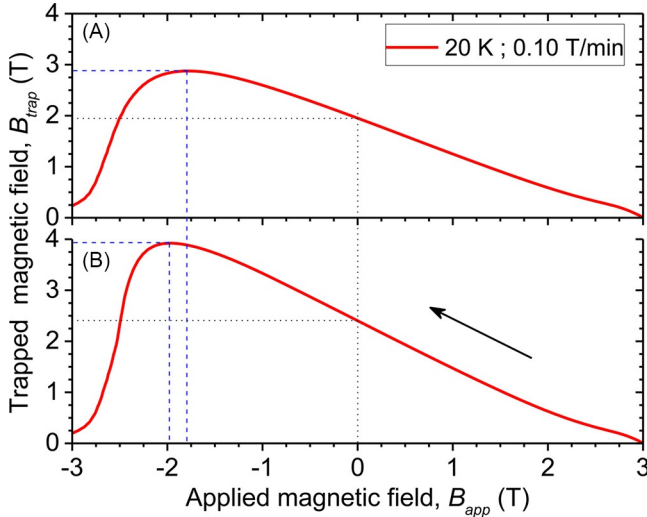
68%, while those of S3 and S4 are 76 and 85%, respectively. The second explanation is the enhancement of vortex pinning resulting from the narrow grains size of S3 and S4. In self-field at 20 K, we have  $J_c = 10^4$  A/cm<sup>2</sup> for S2a,  $J_c = 3.8 \cdot 10^5$  A/cm<sup>2</sup> for S3, and  $J_c = 5 \cdot 10^5$  A/cm<sup>2</sup> for S4.

Fig. 5B shows the real interest of high pressure processing. The  $J_c$  values increase when the processing temperature increases. The maximum temperature of 800°C is due to the mechanical limit of the tungsten carbide mold. In comparison to the sample optimized (950°C, 50 MPa) using a graphite mold, the  $J_c$  values seem to be quite close at 0 T. However, when the applied magnetic field increases, the  $J_c$  values of the samples prepared applying high pressure are higher than that of the sample fabricated with the graphite mold. At 3 T and 20 K, we measure  $J_c = 3.5 \cdot 10^3$  and  $J_c = 4 \cdot 10^4$  A/cm<sup>2</sup> for the samples consolidated at 800°C and 500 MPa, and 950°C and 50 MPa, respectively. This is probably correlated to the bulk density of the sample (see Table 2).

Fig. 6 shows the field trapped by sample S2b at 20 K as a function of the applied external magnetic field. The measurements were achieved with

**Table 2** Processing conditions and bulk density versus pressure

Sample	S2b	S5	S6	S7
mold	Graphite	WC	WC	WC
Temperature (°C)	950	800	750	700
Pressure (MPa)	50	500	500	500
Bulk density (%)	80	96	89	64



**Fig. 6** Trapped field measurements of sample S2b on the top of a 20 mm diameter disk-shaped stack (A) and between them (B).

sensors located (i) on the top of the stack (Fig. 6A) and (ii) between the two disks (Fig. 6B). The results show that the maximal fields ( $B_{\text{trap}}$ ) trapped on the top and between the disks are 2.88 T and 3.92 T under negative supporting field of  $-1.8$  T and  $-1.98$  T, respectively. The remanent magnetic fields  $B_{\text{rem}}$ , defined as the trapped magnet field when the applied field is zero, are equal to 1.95 T and 2.40 T, respectively. Similar results have been reported in the literature and are very promising for the intended applications of bulk  $\text{MgB}_2$  magnets.

Another main functional property for applications is the magnetic levitation force ( $F_L$ ). A new set of disk samples (Table 3) was prepared using the commercial powder.

The samples were measured according to the experimental procedure described elsewhere [48]. However, it should be noted that all measurements were made with a gap  $\sim 8$  mm between the superconductor (located

**Table 3**  $\text{MgB}_2$  discs with various diameters and thicknesses

Sample	H715	H706	H713	H714	H705	H716
Diameter (mm)	20	30	30	30	40	50
Thickness (mm)	10	10	5	3	10	10

The samples were all sintered at  $1000^\circ\text{C}$ , 50 MPa, 20 min

inside the cryostat) and the permanent magnet (located outside). The levitation force is a consequence of the Meissner effect [49]. Basically, the measured levitation is proportional to the magnetic moment,  $m$ , generated by the currents flowing in the sample and to the magnetic field gradient along the axis of the superconductor, according to the equation reported below:

$$F_L = m \frac{\partial B}{\partial z} \quad (2)$$

For this study, two main parameters were investigated: (i) the magnetic levitation force versus the sample diameter, and (ii) the effect of the thickness of the superconductor. The measurements were made in zero field cooling.

Fig. 7A shows the magnetic levitation force,  $F_L(z)$  at 20 K for disks with diameters: 20, 30, 40, and 50 mm with a given sample thickness of 10 mm. We observe that  $F_L$  increases when the sample diameter increases. This is clearly related to the larger current loops in the larger samples, which is related to their magnetic moment [50]. The levitation force of 90 N is measured at a distance of superconductor–permanent magnet of 10 mm. Extrapolating the results after fitting the experimental data, we have calculated  $F_L = 175$  N at 4 mm, corresponding to a magnetic levitation pressure of  $9 \text{ N/cm}^2$ . This value is comparable to the pressure of  $7 \text{ N/cm}^2$  reported elsewhere [51] and shows that bulk  $\text{MgB}_2$  could be a viable variant for magnetic levitation applications. Otherwise, Fig. 7B shows the levitation force of samples with different thicknesses. The figure shows clearly that there is no significant effect of the thickness, the same values of about 30 N at 20 K being measured on disks with thicknesses of 3, 5, and 10 mm respectively. We can conclude that, for levitation applications, thick samples will not be necessary, but large diameters will increase the size of the current loops and, consequently, the values of the levitation forces.

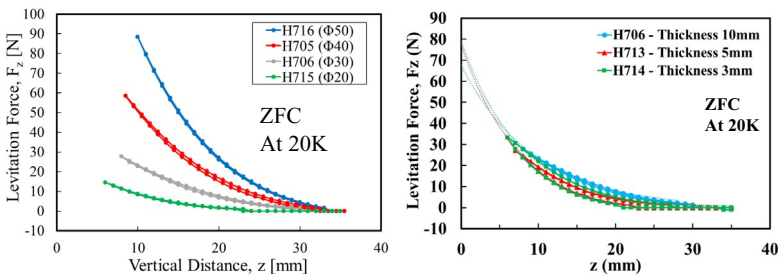


Fig. 7 Magnetic levitation forces at 20K for (A) samples with different diameters and (B) various thicknesses.

**Table 4** Samples prepared at different sintering temperatures, during 20 min and 50 MPa pressure

Sample	H668	H669	H670	E117
Sintering temperature (°C)	950	1000	1100	1200
Density (%)	68.9	78.3	98	98.7

Finally, a last batch of samples was prepared (Table 4) for estimating the mechanical properties.

The knowledge of their mechanical properties is essential for the estimation of the reliability of MgB<sub>2</sub> bulk materials for practical applications. We tested the hardness ( $Hv$ ) of the samples. Basically, the hardness of the samples for an indentation depth,  $h$ , can be calculated from the following equation:

$$Hv = \frac{P_{max}}{A} \quad (3)$$

where  $P_{max}$  refers to the load measured at the maximum penetration depth,  $Hv_{max}$ , while  $A$  refers to the projected contact area (see the insert, Fig. 8) between the indenter and the sample at  $P_{max}$ .

Fig. 8 shows the Vickers hardness,  $Hv$ , of the samples (diameter 20 mm) elaborated by applying 50 MPa during 20 min at 950, 1000, 1100, and 1200°C, respectively. The load was applied parallel to SPS compression direction. The Vickers hardness,  $Hv$ , rises from 200 HV for the sample

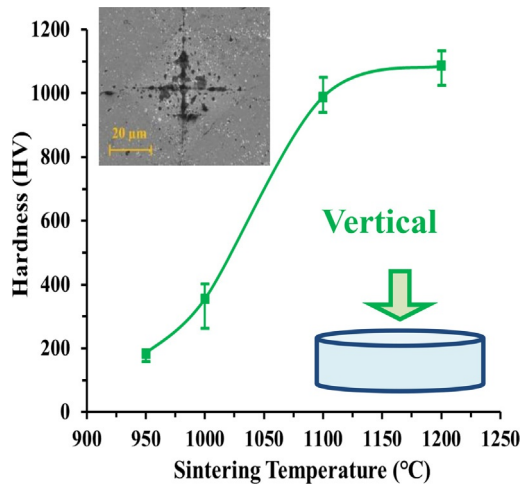


**Fig. 8** Vickers hardness of the samples prepared at different temperatures. (Insert) pattern of the indentation on top surface of the disc sample.

prepared at 950°C to 1100HV for the disc consolidated at 1200°C. The hardness is more than 5 times larger when the bulk density increases from 69% to 99%, as a consequence of a higher processing temperature. This value of 1100HV is significantly larger than the hardness of steel, demonstrating that MgB<sub>2</sub> bulk material is a good candidate for high-speed superconducting flywheels.

### 3.2 Bi<sub>2</sub>Ca<sub>2</sub>Sr<sub>2</sub>CuO<sub>8</sub> superconductor ceramics SPS densified

The SEM image in Fig. 9 shows the fractured cross section of one of the Bi2212 samples. As could be expected from the diffraction patterns, we observe a high degree of orientation of large platelets compactly stacked (98% relative density) along the compression direction of SPT (Fig. 9A) that corresponds to the mean crystallographic *c*-axis. This is in contrast to non-pressed samples (Fig. 9B) in which much smaller platelets appear to be randomly distributed [12] and loosely assembled, resulting in a weak relative density (60%). From magnetic moment and electrical resistivity measurements, the superconducting critical temperature was found equal to 85 K. Magnetic hysteresis cycles were measured at 20 K.

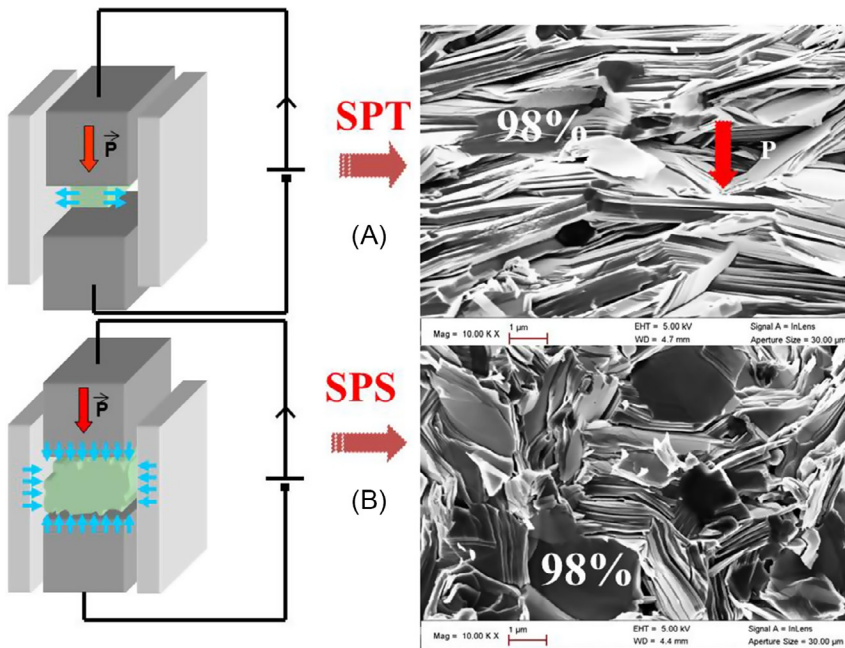
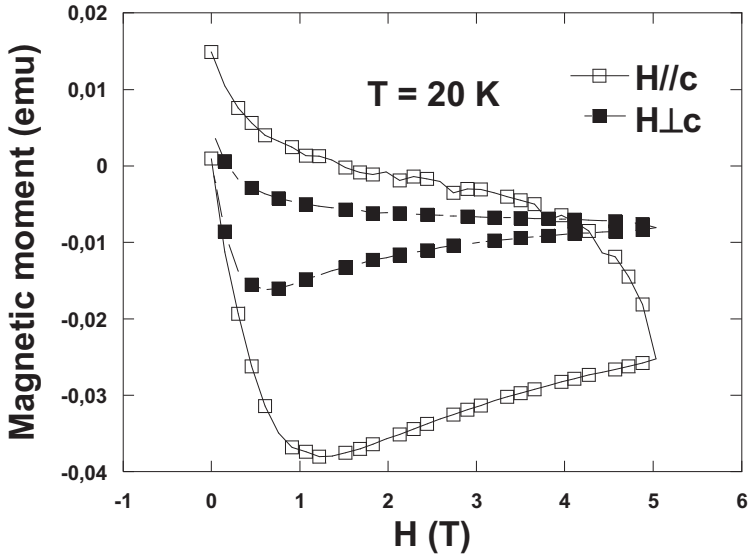


Fig. 9 (A) Spark plasma sintering and (B) texturing versus SEM images.



**Fig. 10** Magnetic moment hysteresis cycles at 20K, the magnetic field,  $H$  is applied in-planes ( $H//c$ ) or out-of-planes ( $H\perp c$ ) showing an anisotropy of the magnetic moment.

**Fig. 10** shows the magnetic moment hysteresis cycles measured carried out on a  $2 \times 2 \times 2 \text{ mm}^3$  specimen cut out from a bulk sample. The excitation field,  $H$ , is either parallel or perpendicular to the direction of the pressure,  $P$ , applied during processing. The hysteresis of the cycle measured with  $H$  parallel to the stress direction is larger than that of the other cycle ( $\Delta M_{H//c} > \Delta M_{H\perp c}$ ). At 1 T; the magnetic moment anisotropy ratio is around 2.

#### 4. Conclusion and outlook

The conclusions that can be drawn from this work are as follows:

- Fast heating spark plasma sintering/texturing (SPS/SPT) allows preparation of dense and textured bulk materials with good superconducting properties.
- The control of the starting powder allowed us to improve the critical current density. At 20 K,  $J_c = 210^5 \text{ A/cm}^2$  in self field and  $J_c \approx 10^5 \text{ A/cm}^2$  with 1 T applied fields have been measured.
- An encouraging trapped field value of 3.9 T at 20 K was obtained on 20 mm diameter disc.

- The levitation force did not depend on the thickness of the samples measured and increased with their diameter. Extrapolating the result of the measurements suggests that a 175 N levitation force can be obtained at 4 mm from a permanent magnet at 20 K with a 50 mm diameter sample. This levitation force corresponds to a  $9\text{ N/cm}^2$  pressure.
- First measurements of the mechanical properties of  $\text{MgB}_2$  samples have shown that their hardness is almost twice that of steel.

## Acknowledgments

This work was partially supported by the French National Research Agency (Agence Nationale de la Recherche-ANR) through the ANR-RESUM (ANR-14-ASTR-009-02). The authors thank Mr. J. Lecourt, C. Bilot, and M. Strebel for their relevant technical supports.

## References

- [1] K. Onnes, Leiden Comm. 120b, 124c (1911).
- [2] J.G. Bednorz, K.A. Müller, Z. Phys. B64 (1984) 189–193.
- [3] H. Maeda, Y. Tanaka, M. Fukutomi, T. Asano, Jpn. J. Appl. Phys. 27 (1988) L209–L210.
- [4] J.M. Tarascon, W.R. McKinnon, P. Barboux, D.M. Hwang, B.G. Bagley, L.H. Greene, G.W. Hull, Y. Lepage, N. Stoffel, M. Giroud, Phys. Rev. B 38 (1988) 8885–8892.
- [5] M. Monteverde, M. Núñez-Regueiro, C. Acha, K.A. Lokshin, D.A. Pavlov, S.N. Putilin, E.V. Antipov, Physica C 408–410 (2004) 23–24.
- [6] J. Nagamatsu, N. Nakagawa, T. Muranaka, Y. Zenitani, J. Akimitsu, Nature 410 (2001) 63–64.
- [7] Y. Mizuguchi, F. Tomioka, S. Tsuda, T. Yamaguchi, Y. Takano, Appl. Phys. Lett. 94 (2009) 012503.
- [8] H. Takahashi, K. Igawa, K. Arii, Y. Kamihara, M. Hirano, H. Hosono, Nature (London) 453 (2008) 376.
- [9] M. Somayazulu, M. Ahart, A.K. Mishra, Z.M. Geballe, M. Baldini, Y. Meng, V.V. Struzhkin, R.J. Hemley, Phys. Rev. Lett. 122 (2019) 027001.
- [10] D. Kenfaui, P.-F. Sibeud, E. Louradour, X. Chaud, J.G. Noudem, Adv. Funct. Mat 24 (2014) 3996–4004.
- [11] N.H. Babu, Y. Shi, K. Iida, D.A. Cardwell, Nat. Mater. 4 (2005) 476–480.
- [12] J.G. Noudem, J. Beille, D. Bourgault, R. Tournier, Physica C 264 (1996) 325.
- [13] T. Sasaki, T. Naito, H. Fujishiro, Phys. Procedia 45 (2013) 93.
- [14] E.A. Goodilin, E.S. Reddy, J.G. Noudem, M. Tarka, G.J. Schmitz, J. Cryst. Growth 241 (2002) 512.
- [15] A. Yamamoto, A. Ishihara, M. Tomita, K. Kishio, Appl. Phys. Lett. 105 (2014) 032601.
- [16] X. Chaud, J. Noudem, T. Prikhna, Y. Savchuk, E. Haanappel, P. Diko, C.P. Zhang, Physica C 469 (2009) 1200–1206.
- [17] J.H. Durrell, C.E.J. Dancer, A. Dennis, Y. Shi, X. Z, A.M. Campbell, N. Hari Babu, R. I. Todd, C.R.M. Grovenor, D.A. Cardwell, Supercond. Sci. Technol. 25 (2012) 112002.
- [18] S. Gruss, G. Fuchs, G. Krabbes, P. Verges, G. Stöver, K.-H. Müller, J. Fink, L. Schultz, Appl. Phys. Lett. 79 (2001) 3131.



- [19] M. Tomita, M. Murakami, *Nature* 421 (2003) 517–520.
- [20] G. Fuchs, P. Schatzle, G. Krabbes, S. Grub, P. Verges, K.-H. Muller, J. Fink, L. Schultz, *Appl. Phys. Lett.* 76 (2000) 2107–2109.
- [21] F.N. Werfel, U. Floegel-Delor, R. Rothfeld, T. Riedel, B. Goebel, D. Wippich, P. Schirrmeister, *Supercond. Sci. Technol.* 25 (2012) 014007.
- [22] G.G. Sotelo, D.H.N. Dias, E.S. Motta, F. Sass, A.C. Ferreira, R. de Andrade Jr., R. M. Stephan, *Phys. Procedia* 36 (2012) 943–947.
- [23] B. Dolisy, S. Mezani, T. Lubin, J. L ev eque, *Supercond. Sci. Technol.* 30 (2017) 35015.
- [24] T. Yanamoto, M. Izumi, M. Yokoyama, K. Umamoto, *Proc. IEEE* 103 (2015) 2333–2343.
- [25] M. Muralidhar, A. Ishihara, K. Suzuki, Y. Fukumoto, Y. Yamamoto, M. Tomita, *Physica C* 494 (2013) 85–88.
- [26] L. Zhou, P. Zhang, P. Ji, K. Wang, J. Wang, X. Wu, *Supercond. Sci. Technol.* 3 (1990) 490.
- [27] S. Jin, T.H. Tiefel, R.C. Sherwood, R.B. van Dover, M.E. Davis, G.W. Kammlott, R. A. Fastnacht, *Phys. Rev. B* 37 (1988) 7850.
- [28] D. Zhou, S. Hara, B. Li, J. Noudem, M. Izumi, *Supercond. Sci. Technol.* 27 (2014) 044015.
- [29] E. Guilmeau, D. Chateigner, J.G. Noudem, *Supercond. Sci. Technol.* 15 (2002) 1436.
- [30] D. Bourgault, J.M. Barbut, J. Ayache, D. Chateigner, R. Tournier, F.J. Gotor, C. Bahezre, P. Germi, M. Pernet, *Physica C* 235–240 (1994) 567–570.
- [31] A. Yamamoto, A. Ishihara, M. Tomita, K. Kishio, *Appl. Phys. Lett.* 105 (2014) 032601.
- [32] Y. Liu, Y. Lin, Z. Shi, C.-W. Nan, Z. Shen, *J. Am. Ceram. Soc.* 88 (2005) 1337–1340.
- [33] M. Tokita, *Mater. Sci. Forum* 492/493 (2005) 711–718.
- [34] M. Suganuma, Y. Kitagawa, S. Wada, N. Murayama, *J. Am. Ceram. Soc.* 86 (2003) 387–394.
- [35] M. Tokita, *Mater. Sci. Forum* 83 (1999) 308–311.
- [36] R. Orru, R. Licheri, A.M. Locci, A. Cincotti, G. Cao, *Mater. Sci. Eng. R* 63 (2009) 127.
- [37] M. Muralidhar, N. Kenta, M.R. Koblischka, M. Murakami, *Phys. Status Solidi A* 212 (10) (2015) 2141–2145.
- [38] J.G. Noudem, *J. Eur. Ceram. Soc.* 29 (2009) 2659–2663.
- [39] J.G. Noudem, D. Kenfaui, D. Chateigner, M. Gomina, *Scr. Mater.* 66 (2012) 258–260.
- [40] C.P. Bean, *Rev. Mod. Phys.* 36 (1964) 31–39.
- [41] K. Berger, M.R. Koblischka, B. Douine, J. Noudem, P. Bernstein, T. Hauet, J. L ev eque, *IEEE Trans. Appl. Supercond.* 26 (3) (2016) 1–5.
- [42] V. Grinenko, E.P. Krasnoperov, C.A. Stolarov, A.A. Bush, B.P. Mikhajlov, *Solid State Commun.* 138 (2006) 461.
- [43] C.E.J. Dancer, D. Prabhakaran, M. Basoglu, E. Yanmaz, H. Yan, M. Reece, R.I. Todd, C.R.M. Grovenor, *Supercond. Sci. Technol.* 22 (2009) 095003.
- [44] Y. Zhao, Y. Feng, C.H. Cheng, L. Zhou, Y. Wu, T. Machi, Y. Fudamoto, N. Koshizuka, M. Murakami, *Appl. Phys. Lett.* 79 (8) (2001) 1154–1156.
- [45] J.-K. Park, U.-I. Chung, N.M. Hwang, D.-Y. Kim, *J. Am. Ceram. Soc.* 84 (12) (2001) 3057–3059.
- [46] N. Rogado, M.A. Hayward, K.A. Regan, Y.Y. Wang, N.P. Ong, H.W. Zandbergen, J.M. Rowell, R.J. Cava, *J. Appl. Phys.* 91 (2002) 274.
- [47] S. Kim, D.S. Stone, J.-I. Cho, C.-Y. Jeong, C.-S. Kang, J.-C. Bae, *J. Alloys Compd.* 470 (2009) 85.
- [48] P. Bernstein, L. Colson, L. Dupont, J. Noudem, *Supercond. Sci. Technol.* 31 (015008) (2018).
- [49] W. Meissner, R. Ochsenfeld, *Naturwissenschaften* 21 (1933) 787.
- [50] E.H. Brandt, *Phys. Rev.* 58 (1998) 6506.
- [51] E. Perini, E. Bassani, G. Giunchi, *Adv. Cryog. Eng.* 55 (2010) 261.